

## SOME MULTISCALE RESULTS USING LIMITED GLOBAL INFORMATION FOR TWO-PHASE FLOW SIMULATIONS

LIJIAN JIANG, JØRG E. AARNES, AND YALCHIN EFENDIEV

**Abstract.** In this paper, we present the analysis of recently introduced multiscale finite element methods that employ limited global information. In particular, these methods use single-phase flow information for the construction of more accurate solution for two-phase immiscible flow dynamics in heterogeneous porous media. We consider the analysis of Galerkin multiscale finite element method as well as mixed multiscale finite element method. Our analysis assumes that the fine-scale features of two-phase flow dynamics strongly depend on single-phase flow. Under this assumption, we present the analysis of multiscale finite element methods that use single-phase flow information. Numerical results are presented which demonstrate that MsFEM using limited global information is more accurate and converges as the coarse mesh size decreases.

**Key Words.** Galerkin multiscale finite element method, mixed multiscale finite element method, global information, two-phase flows

### 1. Introduction

Subsurface flows are often affected by heterogeneities in a wide range of length scales. It is therefore difficult to resolve numerically all of the scales that impact transport. Typically, upscaled or multiscale models are employed for such systems. The main idea of upscaling techniques is to form coarse-scale equations with a prescribed analytical form that may differ from the underlying fine-scale equations. In multiscale methods, the fine-scale information is carried throughout the simulation and the coarse-scale equations are generally not expressed analytically, but rather formed and solved numerically.

Our purpose in this paper is to analyze multiscale finite element methods for two-phase immiscible flows that employ single-phase flow information. A multiscale finite element method was first introduced in [19] and takes its origin from the pioneering work [9]. Its main idea is to incorporate the small-scale information into finite element basis functions and capture their effect on the large scale via finite element computations. The multiscale method in [19] shares some similarities with a number of multiscale numerical methods, such as residual free bubbles [10, 26], variational multiscale method [20], two-scale finite element methods [25], two-scale conservative subgrid approaches [4]. We remark that special basis functions in finite element methods have been used earlier in [9, 7]. The multiscale finite element methodology has been modified and successfully applied to two-phase flow simulations in [21, 13, 1] and extended to nonlinear partial differential equations [18, 17].

---

Received by the editors October 1, 2008 and, in revised form, March 17, 2009.  
2000 *Mathematics Subject Classification.* 65N30, 34E13, 34K28.

Recently, a number of upscaling and multiscale approaches that employ single-phase flow information in upscaling two-phase flow problems have been introduced. For example, in [12], the authors propose adaptive local-global technique that employs the solution of single-phase flow problem for computation of accurate up-scaled properties. In [1] and later in [16], the single-phase flow solution is used to construct multiscale basis functions for accurate simulations of two-phase flow equations. The goal of this paper is to provide analysis of two multiscale finite element methods that use single-phase flow information to construct basis functions. These multiscale techniques have advantages if the fine-scale features of two-phase flow dynamics strongly depend on single-phase flow. In particular, we assume that two-phase flow pressure dynamics strongly depends on single-phase flow pressure. This assumption is shown for channelized permeability in [16]. The convergence rate of multiscale finite element method is obtained under this assumption. We analyze both Galerkin multiscale finite element method as well as mixed multiscale finite element method.

In the paper, we present numerical results which demonstrate that MsFEM using limited global information is more accurate compared to MsFEM which only uses local information to construct basis functions. Moreover, MsFEM with limited global information converges as the coarse mesh size decreases. In our numerical results, the permeability fields from SPE Comparative Solution Project [15] (also known as SPE 10) is used. These permeability fields have channelized structure and a large contrast. Because of channelized structure of the permeability fields, the localized approaches do not perform well. Our numerical results show that one can achieve high accuracy if MsFEM with limited global information is used.

The paper is organized as follows. In the next section, we present a brief discussion of two-phase flow and single-phase flow equations and a brief description of main results. Section 3 is devoted to the analysis of Galerkin multiscale finite element method. In Section 4, we present analysis for mixed multiscale finite element method. In section 5, we present numerical results.

## 2. Motivation

In this section, we briefly present single-phase and two-phase flow equations neglecting the effects of gravity, compressibility, capillary pressure and dispersion on the fine scale. Porosity, defined as the volume fraction of the void space, will be taken to be constant and therefore serves only to rescale time. The two phases will be referred to as water and oil and designated by the subscripts  $w$  and  $o$ , respectively. We can then write Darcy's law, with all quantities dimensionless, for each phase  $j$  as follows:

$$(1) \quad \mathbf{v}_j = -\lambda_j(S)k\nabla p,$$

where  $\mathbf{v}_j$  is phase velocity ( $j = w, o$ ),  $S$  is water saturation (volume fraction),  $p$  is pressure,  $\lambda_j = k_{rj}(S)/\mu_j$  is phase mobility, where  $k_{rj}$  and  $\mu_j$  are the relative permeability and viscosity of phase  $j$  respectively, and  $k$  is the permeability tensor, which is here taken to be diagonal.

Combining Darcy's law with conservation of mass,  $div(\mathbf{v}_w + \mathbf{v}_o)=0$ , allows us to write the flow equation in the following form

$$(2) \quad div(\lambda(S)k\nabla p) = f,$$

where the total mobility  $\lambda(S)$  is given by  $\lambda(S) = \lambda_w(S) + \lambda_o(S)$  and  $f$  is the source term which represents wells. The saturation dynamics affects the flow equations.

One can derive the equation describing the dynamics of the saturation

$$(3) \quad \frac{\partial S}{\partial t} + \operatorname{div}(\mathbf{F}) = 0,$$

where  $\mathbf{F} = \mathbf{v}f(S)$ , with  $f(S)$ , the fractional flow of water, given by  $f = \lambda_w/(\lambda_w + \lambda_o)$ , and the total velocity  $\mathbf{v}$  by:

$$(4) \quad \mathbf{v} = \mathbf{v}_w + \mathbf{v}_o = -\lambda(S)k\nabla p.$$

In the presence of capillary effects, an additional diffusion term is present in (3).

For the case of single-phase flow and unit mobility ratio, we have  $k_{rw} = S$ ,  $k_{ro} = 1 - S$  and  $\mu_w = \mu_o$ . As a result,  $\lambda(S) = 1/\mu_w = 1/\mu_o$ ,  $f(S) = S$  and the flow equation reduces to

$$\operatorname{div}(k\nabla p^{sp}) = f.$$

The saturation equation reduces to the linear advection pollutant transport equation.

As mentioned in Introduction, for the analysis of multiscale finite element methods, we will assume that the fine-scale features of two-phase flow strongly depend on single-phase flow in each coarse block. We stress that our goal is to understand mathematically, and find sufficient conditions when single-phase flow based multiscale methods are accurate. Since rigorous theory of two-phase flow dynamics is not well understood, we resort to assumptions to justify the efficiency of single-phase flow based multiscale methods.

Next, we briefly describe some of our main results and assumptions. As shown in [16], the pressure equation can be written in a coordinate system defined by the streamfunction  $\psi$  and the pressure  $p$  at initial time; i.e.,  $\eta = \psi(\mathbf{x}, t = 0)$  and  $\zeta = p(\mathbf{x}, t = 0) = p^{sp}(\mathbf{x})$ . We restrict ourselves to two dimensions. Then the equation for the pressure can be written in the  $(\eta, \zeta)$  coordinate system as

$$(5) \quad \frac{\partial}{\partial \eta} \left( k^2 \lambda(S) \frac{\partial p}{\partial \eta} \right) + \frac{\partial}{\partial \zeta} \left( \lambda(S) \frac{\partial p}{\partial \zeta} \right) = 0.$$

Assuming that the permeability has strong channelized feature and the variation within the channel (in the  $\eta$  direction) is weak, that  $S = 0$  at initial time, and that the imposed global boundary conditions result in high flow within the channel (this is fairly typical), it was shown in [16] that

$$p(\eta, \zeta, t) = \hat{p}(\zeta, t) + \text{high order terms},$$

where  $\hat{p}(\zeta, t)$  is the dominant pressure. Note that this result is shown when  $\lambda$  is smooth. This result indicates that the pressure (which varies in time due to saturation effects) depends strongly on the initial pressure  $\zeta$ ; i.e., the leading order term in the asymptotic expansion is a function of initial pressure and time only. Our main assumption is that the two-phase flow pressure at any time satisfies:

$$(6) \quad p(\mathbf{x}, t) = \hat{p}(p^{sp}, t) + \text{high order terms}.$$

We note that (6) does not hold when  $\lambda$  has discontinuities. In this case, our results hold away from the sharp interfaces and one can localize the interface by updating some basis functions. Our numerical results show that this update does not improve the results substantially. We believe this is because that the jump discontinuities in  $\lambda$  is small compared to heterogeneities in porous media, the effects of which we capture using limited global information.

Next, we briefly present a numerical results to demonstrate the efficiency of the proposed approach. In Table 1, the relative  $L_1$  errors of the saturation are compared for MsFEM with global information and MsFEM which does not use limited

global information. Our fine-scale field is  $60 \times 220$  and the permeability fields are taken from SPE Comparative Solution Project [15] (also known as SPE 10). These permeability fields have channelized structure and difficult to upscale. One can see from this table that MsFEM using limited global information is more accurate and converges as the coarse mesh size decreases. On contrary, MsFEM which only uses local information does not converge as the coarse mesh size decreases, The details of the numerical results can be found in Section 5.

TABLE 1. Relative saturation errors (layer=40,  $\frac{\mu_w}{\mu_o} = 1/3$ )

coarse grid	saturation error (global)	saturation error (local)
$6 \times 10$	0.0512	0.2755
$12 \times 11$	0.0435	0.3459
$12 \times 22$	0.0370	0.3158

### 3. Galerkin multiscale finite element methods

**3.1. Galerkin multiscale finite element method with limited global information.** The key idea of the method is the construction of basis functions on coarse grids that capture small-scale information. The basis functions are constructed from the solution of the leading order homogeneous elliptic equation on each coarse element with some specified boundary conditions. For further analysis,  $K$  denotes a generic coarse element and  $\tau_h$  is a quasi-uniform family of coarse elements. Thus, if we consider a coarse element  $K$  that has  $d$  vertices  $\mathbf{x}_j$ , the local basis functions  $\phi_i, i = 1, \dots, d$  are set to satisfy the following elliptic problem

$$(7) \quad \begin{cases} \operatorname{div}(k(\mathbf{x})\nabla\phi_i^K) = 0 & \text{in } K \\ \phi_i^K = d_i^K & \text{on } \partial K, \\ \phi_i^K(\mathbf{x}_j) = \delta_{ij}, \end{cases}$$

where  $\delta_{ij} = 1$  if  $i = j$  and  $\delta_{ij} = 0$  if  $i \neq j$ .

In previous findings, the function  $d_i^K$  for each  $i$  has been defined in various ways, e.g., it is chosen to vary linearly along  $\partial K$ , or to be the solution of a local one-dimensional problems [21]. A solution of the problem in a slightly larger domain has also been used to define boundary conditions [19]. It can be shown that if  $d_i^K$  varies linearly along  $\partial K$ , then the multiscale finite element method for two-phase flow has a resonance error as in the case of standard multiscale finite element methods (see [19]).

We would like to note that an approximate solution of (7) can be used. For example, in the case of periodic or scale separation cases, the basis functions can be approximated using homogenization expansion (see [16]). This type of simplification is not applicable for problems considered in this paper.

Next, we briefly describe multiscale finite element method using information from a single-phase flow solution. For simplicity, we restrict ourselves to the two dimensional case. For this method,  $d_i^K$  is the linear interpolation of  $p^{sp}$  using the values of  $p^{sp}(\mathbf{x}_j)(j = 1, \dots, d)$  [16]. In particular, for each element  $K$  (see Figure 1) with vertices  $\mathbf{x}_i (i = 1, \dots, d)$  denote by  $\phi_i^K(\mathbf{x})$  a restriction of the nodal basis on  $K$ , such that  $\phi_i^K(\mathbf{x}_j) = \delta_{ij}$ . At the edges where  $\phi_i^K(\mathbf{x}) = 0$  at both vertices, we take boundary condition for  $\phi_i^K(\mathbf{x})$  to be zero. Consequently, the basis functions are localized. We only need to determine the boundary condition at two edges that have the common vertex  $\mathbf{x}_i$  ( $\phi_i^K(\mathbf{x}_i) = 1$ ). Denote these two edges by  $[\mathbf{x}_{i-1}, \mathbf{x}_i]$

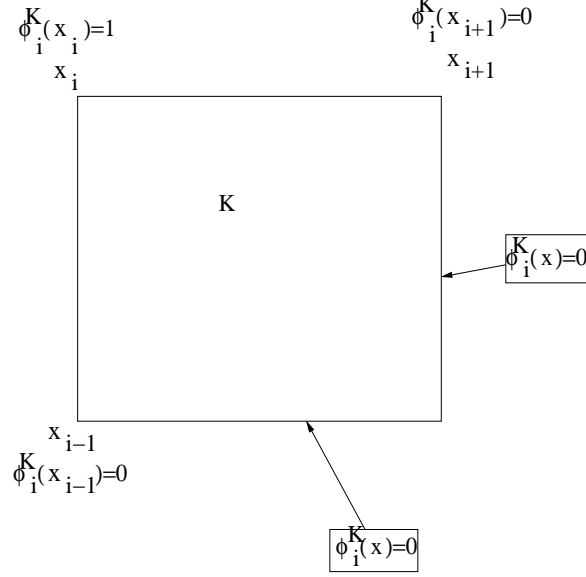


FIGURE 1. Schematic description of basis function

and  $[\mathbf{x}_i, \mathbf{x}_{i+1}]$ . We only need to describe the boundary condition,  $d_i^K$ , for the basis function  $\phi_i^K$ , along the edges  $[\mathbf{x}_i, \mathbf{x}_{i+1}]$  and  $[\mathbf{x}_i, \mathbf{x}_{i-1}]$ . If  $p^{sp}(\mathbf{x}_i) \neq p^{sp}(\mathbf{x}_{i+1})$ , then

$$d_i^K(\mathbf{x})|_{[\mathbf{x}_i, \mathbf{x}_{i+1}]} = \frac{p^{sp}(\mathbf{x}) - p^{sp}(\mathbf{x}_{i+1})}{p^{sp}(\mathbf{x}_i) - p^{sp}(\mathbf{x}_{i+1})}, \quad d_i^K(\mathbf{x})|_{[\mathbf{x}_i, \mathbf{x}_{i-1}]} = \frac{p^{sp}(\mathbf{x}) - p^{sp}(\mathbf{x}_{i-1})}{p^{sp}(\mathbf{x}_i) - p^{sp}(\mathbf{x}_{i-1})}.$$

The case  $p^{sp}(\mathbf{x}_i) = p^{sp}(\mathbf{x}_{i+1}) \neq 0$  and others can also be described (see [16]).

We define the Galerkin finite element space by

$$(8) \quad V_h = \text{span}\{\phi_i^K : 1, \dots, d; K \in \tau_h\}.$$

The weak formulation of (2) is to seek  $p_h \in V_h$  such that

$$(9) \quad (\lambda k \nabla p_h, \nabla q_h) = (f, q_h) \quad \text{for any } q_h \in V_h,$$

where  $(\cdot, \cdot)$  denotes inner product in  $L^2$ . In this case, we have the Cea's estimate [14]

$$(10) \quad |p - p_h|_{1, \Omega} \leq C \inf_{q_h \in V_h} |p - q_h|_{1, \Omega},$$

where  $p$  is the solution of two-phase flow (2) and  $p_h$  is the numerical solution defined in (9). Throughout, we denote by  $\|\cdot\|_{m, \Omega}$  and  $|\cdot|_{m, \Omega}$   $H^m(\Omega)$  norm and semi-norm, respectively and  $C$  denotes a generic constant independent of mesh size. Using (10), one can show  $p_h^{sp} = p^{sp}$  in each coarse block  $K$  (see [16]) for the case with zero source term and non-zero boundary conditions. If the source term is not zero and in  $L_2(\Omega)$ , it can be easily shown that  $|p_h^{sp} - p^{sp}|_{1, \Omega} \leq Ch\|f\|_{0, \Omega}$ .

**3.2. Error analysis for Galerkin MsFEM.** We will use the following assumption.

*Assumption G.* There exists  $G(\eta)$  sufficiently smooth ( $G \in W^{3, \frac{2s}{s-4}}$ ,  $s > 4$ ), such that

$$(11) \quad |p - G(p^{sp})|_{1, \Omega} \leq C\delta,$$

where  $\delta$  is sufficiently small.

Note that  $G$  is defined on a bounded interval because  $p^{sp}$  is a bounded function.

Following standard practice of finite element estimation, we seek  $q_h = c_i \phi_i^K$ , where  $\phi_i^K$  are single-phase flow based multiscale finite element basis functions. Throughout the paper, we assume there is a summation over repeated indices. Then from (10), we have

$$(12) \quad |p - p_h|_{1,\Omega} \leq |p - G(p^{sp})|_{1,\Omega} + |G(p^{sp}) - c_i \phi_i^K|_{1,\Omega}.$$

Next, we present an estimate for the second term. We choose  $c_i = G(p^{sp}(\mathbf{x}_i))$ , where  $\mathbf{x}_i$  are vertices of  $K$ . Furthermore, using Taylor expansion of  $G$  around  $\bar{p}_K$ , which is the average of  $p^{sp}$  over  $K$ ,

$$(13) \quad \begin{aligned} G(p^{sp}(\mathbf{x}_i)) &= G(\bar{p}_K) + G'(\bar{p}_K)(p^{sp}(\mathbf{x}_i) - \bar{p}_K) \\ &+ (p^{sp}(\mathbf{x}_i) - \bar{p}_K)^2 \int_0^1 s G''(p^{sp}(\mathbf{x}_i) + s(\bar{p}_K - p^{sp}(\mathbf{x}_i))) ds. \end{aligned}$$

Then we have in each  $K$ ,

$$(14) \quad \begin{aligned} c_i \phi_i^K &= G(\bar{p}_K) \sum_i \phi_i^K + G'(\bar{p}_K)(p^{sp}(\mathbf{x}_i) - \bar{p}_K) \phi_i^K \\ &+ (p^{sp}(\mathbf{x}_i) - \bar{p}_K)^2 \phi_i^K \int_0^1 s G''(p^{sp}(\mathbf{x}_i) + s(\bar{p}_K - p^{sp}(\mathbf{x}_i))) ds \\ &= G(\bar{p}_K) + G'(\bar{p}_K)(p^{sp}(\mathbf{x}_i) \phi_i^K - \bar{p}_K) \\ &+ (p^{sp}(\mathbf{x}_i) - \bar{p}_K)^2 \phi_i^K \int_0^1 s G''(p^{sp}(\mathbf{x}_i) + s(\bar{p}_K - p^{sp}(\mathbf{x}_i))) ds. \end{aligned}$$

In the last step, we have used  $\sum_i \phi_i^K = 1$ . Similarly, in each  $K$ ,

$$(15) \quad \begin{aligned} G(p^{sp}(\mathbf{x})) &= G(\bar{p}_K) + G'(\bar{p}_K)(p^{sp}(\mathbf{x}) - \bar{p}_K) \\ &+ (p^{sp}(\mathbf{x}) - \bar{p}_K)^2 \int_0^1 s G''(p^{sp}(\mathbf{x}) + s(\bar{p}_K - p^{sp}(\mathbf{x}))) ds. \end{aligned}$$

Using (14) and (15), we get

$$(16) \quad \begin{aligned} |G(p^{sp}) - c_i \phi_i^K|_{1,K} &\leq |G'(\bar{p}_K)(p^{sp}(\mathbf{x}) - p^{sp}(\mathbf{x}_i) \phi_i^K)|_{1,K} \\ &+ |(p^{sp}(\mathbf{x}_i) - \bar{p}_K)^2 \phi_i^K \int_0^1 s G''(p^{sp}(\mathbf{x}_i) + s(\bar{p}_K - p^{sp}(\mathbf{x}_i))) ds|_{1,K} \\ &+ |(p^{sp}(\mathbf{x}) - \bar{p}_K)^2 \int_0^1 s G''(p^{sp}(\mathbf{x}) + s(\bar{p}_K - p^{sp}(\mathbf{x}))) ds|_{1,K}. \end{aligned}$$

Since  $|p^{sp}(\mathbf{x}) - p^{sp}(\mathbf{x}_i) \phi_i^K|_{1,K} \leq Ch \|f\|_{0,K}$ , the estimate of the first term is the following

$$|G'(\bar{p}_K)(p^{sp}(\mathbf{x}) - p^{sp}(\mathbf{x}_i) \phi_i^K)|_{1,K} \leq Ch \|f\|_{0,K}.$$

For the second term on the right hand side of (16), assuming  $p^{sp}(\mathbf{x}) \in W^{1,s}(\Omega)$  ( $s > 4$ ), we have

$$(17) \quad \begin{aligned} &|(p^{sp}(\mathbf{x}_i) - \bar{p}_K)^2 \phi_i^K \int_0^1 s G''(p^{sp}(\mathbf{x}_i) + s(\bar{p}_K - p^{sp}(\mathbf{x}_i))) ds|_{1,K} \\ &\leq Ch |p^{sp}|_{1,4,K}^2 |p^{sp}|_{1,K} \\ &\leq Ch |p^{sp}|_{1,4,K}^2. \end{aligned}$$

where we have used the assumption  $|\phi_i^K|_{1,K} \leq C$  and the Sobolev space imbedding  $W^{1,s} \subset W^{1,4}$  ( $s > 4$ ). Here, we have used the inequality (e.g., [3])

$$|u(\mathbf{x}) - u(\mathbf{y})| \leq C |\mathbf{x} - \mathbf{y}|^{1-2/s} |u|_{1,s,K}.$$

For the third term on the right hand side of (16), smoothness assumption of  $G$  and a straightforward calculation give rise to

$$\begin{aligned}
& |(p^{sp}(\mathbf{x}) - \bar{p}_K)^2 \int_0^1 sG''(p^{sp}(\mathbf{x}) + s(\bar{p}_K - p^{sp}(\mathbf{x})))ds|_{1,K} \\
& \leq \|(p^{sp}(\mathbf{x}) - \bar{p}_K)^2 \nabla p^{sp}(\mathbf{x}) \int_0^1 (1-s)sG'''(p^{sp}(\mathbf{x}) + s(\bar{p}_K - p^{sp}(\mathbf{x})))ds\|_{0,K} \\
(18) \quad & + \|2(p^{sp}(\mathbf{x}) - \bar{p}_K)\nabla p^{sp}(\mathbf{x}) \int_0^1 sG''(p^{sp}(\mathbf{x}) + s(\bar{p}_K - p^{sp}(\mathbf{x})))ds\|_{0,K} \\
& \leq Ch^{2-2/s}\|\nabla p^{sp}\|_{0,s,K}^3 \|G'''\|_{0,\frac{2s}{s-4},K} + Ch^{1-2/s}|p^{sp}|_{1,s,K}|p^{sp}|_{1,K} \\
& \leq Ch^{2-2/s}\|\nabla p^{sp}\|_{0,s,K}^3 + Ch^{1-2/s}|p^{sp}|_{1,K},
\end{aligned}$$

where we have used Höld inequality in the second step.

Combining the above estimates, we have for (16),

$$(19) \quad |G(p^{sp}) - c_i \phi_i^K|_{1,K} \leq C(h|p^{sp}|_{1,4,K}^2 + h^{2-2/s} + h^{1-2/s}|p^{sp}|_{1,K} + h\|f\|_{0,K}).$$

Summing (19) over all  $K$  and taking into account Assumption G, we have

$$\begin{aligned}
(20) \quad |p - p_h|_{1,\Omega} & \leq C(\delta + h^{1-2/s} + h|p^{sp}|_{1,4,\Omega}^2 + h^{1-2/s}|p^{sp}|_{1,\Omega} + h\|f\|_{0,\Omega}) \\
& \leq C(\delta + h^{1-2/s} + h|p^{sp}|_{1,s,\Omega}^2 + h^{1-2/s}|p^{sp}|_{1,s,\Omega} + h\|f\|_{0,\Omega})
\end{aligned}$$

Consequently, if  $s > 4$  (see e.g., [6]) single-phase flow based multiscale finite element method converges and we have the following theorem.

**Theorem 3.1.** *Under Assumption G and  $p^{sp} \in W^{1,s}(\Omega)$  ( $s > 4$ ), multiscale finite element method converges with the rate given by (20).*

**Remark 3.1.** *We can relax the assumption on G. In particular, it is sufficient to assume  $G \in W^{2,m}$  ( $m \geq 1$ ). In this case, the proof can be carried out using Taylor polynomials in Sobolev spaces. Also, if we assume  $\nabla p^{sp} \in L^\infty(\Omega)$ , then the convergence rate in (20) is  $C\delta + Ch$ .*

**Remark 3.2.** *The multiscale finite element methods considered above employ information from only one single-phase flow solution. In general, depending on the source term, boundary data, and mobility  $\lambda(S)$  (if it contains sharp variations), it might be necessary to use information from multiple global solutions for the computation of accurate two-phase flow solution. The previous multiscale finite element methods can be extended to take into account additional global information. We can utilize the framework of partition of unity method [8] and construct basis function in each ‘‘patch’’ [8] by using multiple global functions. Let  $p_1, p_2, \dots, p_N$  are the global functions such that  $|p - G(p_1, p_2, \dots, p_N)|_{1,\Omega}$  is sufficiently small, then we can show that*

$$|p - p_h|_{1,\Omega} \leq C\delta + Ch^{1-2/s}$$

for the proposed partition of unity method using multiple global functions. The details and proof can be found in [22].

## 4. Mixed multiscale finite element methods

**4.1. Mixed multiscale finite element with limited global information.** For simplicity, we assume Neumann boundary conditions. First, we review the mixed multiscale finite element formulation following [13] (see also [4], [1], and [5]). We

can rewrite two-phase flow equation as

$$(21) \quad \begin{cases} (\lambda k)^{-1} \mathbf{u} - \nabla p = 0 & \text{in } \Omega \\ \operatorname{div}(\mathbf{u}) = 0 & \text{in } \Omega \\ \lambda(\mathbf{x})k(\mathbf{x})\nabla p \cdot \mathbf{n} = g(\mathbf{x}) & \text{on } \partial\Omega. \end{cases}$$

The variational problem associated with (21) is to seek  $(\mathbf{u}, p) \in H(\operatorname{div}, \Omega) \times L^2(\Omega)/R$  such that  $\mathbf{u} \cdot \mathbf{n} = g$  on  $\partial\Omega$  and

$$(22) \quad \begin{aligned} ((\lambda k)^{-1} \mathbf{u}, \mathbf{v}) + (\operatorname{div} \mathbf{v}, p) &= 0 \quad \forall \mathbf{v} \in H_0(\operatorname{div}, \Omega) \\ (\operatorname{div} \mathbf{u}, q) &= 0 \quad \forall q \in L^2(\Omega)/R. \end{aligned}$$

where

$$H_0(\operatorname{div}, \Omega) = \{\mathbf{v} \in H(\operatorname{div}, \Omega) \mid \mathbf{v} \cdot \mathbf{n} = 0\}.$$

By defining

$$(23) \quad a(\mathbf{u}, \mathbf{v}) = ((\lambda k)^{-1} \mathbf{u}, \mathbf{v}), \quad b(\mathbf{v}, q) = (\operatorname{div} \mathbf{v}, q),$$

we can rewrite the weak formulation as

$$\begin{aligned} a(\mathbf{u}, \mathbf{v}) + b(\mathbf{v}, p) &= 0 \quad \forall \mathbf{v} \in H_0(\operatorname{div}, \Omega), \\ b(\mathbf{u}, q) &= 0 \quad \forall q \in L^2(\Omega)/R. \end{aligned}$$

Let  $\mathbf{V}_h \subset H(\operatorname{div}, \Omega)$  and  $Q_h \subset L^2(\Omega)/R$  be finite dimensional spaces and  $\mathbf{V}_h^0 = \mathbf{V}_h \cap H_0(\operatorname{div}, \Omega)$ . The numerical approximation problem associated with (22) is to find  $(\mathbf{u}_h, p_h) \in \mathbf{V}_h \times Q_h$  such that  $\mathbf{u}_h \cdot \mathbf{n} = g_h$  on  $\partial\Omega$ , where  $g_h = \mathbf{g}_{0,h} \cdot \mathbf{n}$  on  $\partial\Omega$  and  $\mathbf{g}_{0,h} = \sum_{e \in \{\partial K \cap \partial\Omega, K \in \tau_h\}} (\int_e g ds) \mathbf{N}_e$ ,  $\mathbf{N}_e \in \mathbf{V}_h$  is corresponding basis function to edge  $e$ ,

$$(24) \quad \begin{aligned} ((\lambda k)^{-1} \mathbf{u}_h, \mathbf{v}_h) + (\operatorname{div} \mathbf{v}_h, p_h) &= 0 \quad \forall \mathbf{v}_h \in \mathbf{V}_h^0 \\ (\operatorname{div} \mathbf{u}_h, q_h) &= 0 \quad \forall q_h \in Q_h. \end{aligned}$$

One can define a linear operator  $B_h : \mathbf{V}_h^0 \rightarrow Q_h'$  by  $b(\mathbf{u}_h, q_h) = (B_h \mathbf{u}_h, q_h)$ .

Suppose that the following conditions are satisfied

$$(25) \quad a(\mathbf{u}_h, \mathbf{u}_h) \text{ is } \ker B_h \text{ - coercive}$$

$$(26) \quad \inf_{q_h \in Q_h} \sup_{\mathbf{v}_h \in \mathbf{V}_h} \frac{b(\mathbf{v}_h, q_h)}{\|\mathbf{v}_h\|_{H(\operatorname{div}, \Omega)} \|q_h\|_{L^2(\Omega)}} \geq C.$$

Then the following approximation property follows (see e.g., [11]).

**Lemma 4.1.** *If  $(\mathbf{u}, p)$  and  $(\mathbf{u}_h, p_h)$  respectively solve the problem (22) and (24) and the conditions (25) and (26) hold, then*

$$(27) \quad \|\mathbf{u} - \mathbf{u}_h\|_{H(\operatorname{div}, \Omega)} + \|p - p_h\|_{0, \Omega} \leq \inf_{\substack{\mathbf{v}_h \in \mathbf{V}_h \\ \mathbf{v}_h - \mathbf{g}_{0,h} \in \mathbf{V}_h^0}} \|\mathbf{u} - \mathbf{v}_h\|_{H(\operatorname{div}, \Omega)} + \inf_{q_h \in Q_h} \|p - q_h\|_{0, \Omega}.$$

Following [13, 4], one can construct multiscale basis functions for velocity in each coarse block  $K$

$$(28) \quad \begin{aligned} \operatorname{div}(k(\mathbf{x})\nabla w_i^K) &= \frac{1}{|K|} \quad \text{in } K \\ k(\mathbf{x})\nabla w_i^K \mathbf{n}^K &= \begin{cases} g_i^K & \text{on } e_i^K \\ 0 & \text{else,} \end{cases} \end{aligned}$$

where  $e_i^K$  are the edges of  $K$ . If  $g_i^K = \frac{1}{|e_i^K|}$ , then we get the standard mixed MsFEM velocity basis  $\Psi_i^K = k(\mathbf{x})\nabla w_i^K$  [13].

Next we present a mixed multiscale finite element method that employs single-phase flow information. Suppose that  $p^{sp}$  solves the single-phase flow equation. We set  $b_i^K = (k\nabla p^{sp}|_{e_i^K}) \cdot \mathbf{n}^K$  and assume that  $b_i^K$  is uniformly bounded. Then the new basis functions for velocity is constructed by solving the following problems (28) with  $g_i^K = b_i^K / \beta_i^K$ , where  $\beta_i^K = \int_{e_i^K} k\nabla p^{sp} \cdot \mathbf{n}^K ds$ . For further analysis, we assume that  $\beta_i^K \neq 0$ . In general, if  $\beta_i^K = 0$  one can use standard mixed multiscale finite element basis functions. Let  $\mathbf{N}_i^K = k(\mathbf{x})\nabla w_i^K$  and the multiscale finite dimensional space  $\mathbf{V}_h^0$  for velocity be defined by

$$\begin{aligned}\mathbf{V}_h &= \bigoplus_K \{\mathbf{N}_i^K\} \subset H(\text{div}, \Omega), \\ \mathbf{V}_h^0 &= \mathbf{V}_h \cap H_0(\text{div}, \Omega).\end{aligned}$$

First, we will show that the resulting multiscale finite element solution for velocity is exact for single-phase flow (i.e.,  $\lambda(\mathbf{x}) = 1$ ). Let  $\mathbf{v}_h|_K = \beta_i^K \mathbf{N}_i^K$ , then  $\beta_i^K$  is the interpolation value of the fine scale solution. Furthermore, a direct calculation yields  $(\mathbf{v}_h|_{e_i^K}) \cdot \mathbf{n}^K = k\nabla p^{sp} \cdot \mathbf{n}^K$ . Since

$$\text{div} \mathbf{v}_h = \beta_i^K \text{div} \mathbf{N}_i^K = \frac{1}{|K|} \int_{\partial K} k\nabla p^{sp} \cdot \mathbf{n}^K ds = \frac{1}{|K|} \int_K \text{div}(k\nabla p^{sp}) dx = 0,$$

the following equation is obtained immediately

$$(29) \quad \text{div} \mathbf{v}_h = 0 \quad \text{in } K$$

$$(30) \quad \mathbf{v}_h \cdot \mathbf{n}^K = k\nabla p^{sp} \cdot \mathbf{n}^K \quad \text{on } \partial K$$

Since  $\text{div}(k\nabla p^{sp}) = 0$ , we get  $\mathbf{v}_h = k\nabla p^{sp}$  and the following proposition.

**Proposition 4.2.** *Let  $\beta_i^K = \int_{e_i^K} k\nabla p^{sp} \cdot \mathbf{n}^K ds$ , then on each coarse block  $K$*

$$(31) \quad k\nabla p^{sp} = \beta_i^K \mathbf{N}_i^K.$$

For the mixed MsFEM using single phase flow information, we assume that (25) and (26) hold. The proof can be found in [22] under some assumptions. We will focus on the approximation analysis in the following subsection. We note that more general analysis results are presented in [2, 23] when  $\delta = 0$  (see 32). In fact, this paper was written before [2, 23].

**4.2. Error analysis.** First, we re-formulate our assumption for the analysis of mixed multiscale finite element methods. From (11), it follows that

$$\|\nabla p - G'(p^{sp})\nabla p^{sp}\|_{0,\Omega} \leq C\delta.$$

Using the fact that  $k$  and  $\lambda(\mathbf{x})$  are bounded, we have

$$\|\lambda(\mathbf{x})k\nabla p - G'(p^{sp})\lambda(\mathbf{x})k\nabla p^{sp}\|_{0,\Omega} \leq C\delta.$$

Noting that  $\mathbf{u} = \lambda(\mathbf{x})k\nabla p$  and  $\mathbf{u}^{sp} = k\nabla p^{sp}$ , it follows that there exists a coarse-scale scalar function  $A(\mathbf{x})$  such that

$$(32) \quad \|\mathbf{u} - A(\mathbf{x})\mathbf{u}^{sp}\|_{0,\Omega} \leq \delta.$$

Since  $A(\mathbf{x})\mathbf{u}^{sp}$  approximates  $\mathbf{u}$ , we assume that it has small divergence,

$$(33) \quad \left| \int_K \text{div}(A(\mathbf{x})\mathbf{u}^{sp}) dx \right| \leq C\delta_1 h^2$$

in each  $K$ , where  $\delta_1$  is a small number. For our analysis, we note that (33) gives

$$(34) \quad \left| \int_{\partial K} A(\mathbf{x})\mathbf{u}^{sp} \mathbf{n}^K ds \right| \leq C\delta_1 h^2.$$

We will assume that  $A(\mathbf{x}) \in C^\gamma$  (Höld continuous function). (34) can be written as

$$(35) \quad \left| \sum_i A_i \int_{e_i^K} \mathbf{u}^{sp} \mathbf{n}^K ds \right| \leq C \delta_1 h^2.$$

Here  $A_i$ 's are defined as  $A_i = \int_{e_i^K} A(\mathbf{x}) \mathbf{u}^{sp} \mathbf{n}^K ds / \int_{e_i^K} \mathbf{u}^{sp} \mathbf{n}^K ds$ , since  $\int_{e_i^K} \mathbf{u}^{sp} \mathbf{n}^K ds = \beta_i^K \neq 0$ . Note that *not* for any  $A(\mathbf{x})$ ,  $A_i$  is necessarily a value of  $A(\mathbf{x})$  along the edge  $e_i^K$  because  $\mathbf{u}^{sp} \mathbf{n}^K$  can change sign. However, we only need to define  $A(\mathbf{x})$  for each edge by its value  $A_i$  (e.g., the value of  $A(\mathbf{x})$  at the center of edge). Then, for any such  $A(\mathbf{x})$ , (32) is satisfied provided  $\delta < h^\gamma$ . This can be directly verified. Thus, our main assumption will be (32) and (35), where  $A(\mathbf{x})$  is defined, for example, at the center of each edge  $e_i^K$ . We would like to note that from the fact that  $\text{div}(A(\mathbf{x}) \mathbf{u}^{sp})$  is small in each  $K$ , it follows that  $A(\mathbf{x})$ , for example, can be taken as an approximation of stream function corresponding to  $\mathbf{u}^{sp}$ .

Next, we present our error analysis. Based on (27), we estimate  $\|\mathbf{u} - c_i^K \mathbf{N}_i\|_{H(\text{div}, \Omega)}$  with appropriate  $c_i^K$ .

$$(36) \quad \|\mathbf{u} - c_i^K \mathbf{N}_i^K\|_{H(\text{div}, \Omega)} \leq \|\mathbf{u} - c_i^K \mathbf{N}_i^K\|_{0, \Omega} + \|\text{div}(c_i^K \mathbf{N}_i^K)\|_{0, \Omega}.$$

Because  $\text{div}(\mathbf{N}_i^K) = 1/|K|$ , the second term is equal to  $\frac{1}{h} (\sum_K |\sum_i c_i^K|^2)^{\frac{1}{2}}$ . Next, we choose  $c_i^K = A_i \beta_i^K$ . Then, noticing that  $\beta_i^K = \int_{e_i^K} \mathbf{u}^{sp} \mathbf{n}^K ds$ , we have from (35)

$$\left| \sum_i c_i^K \right| \leq C \delta_1 h^2$$

for each  $K$ . Consequently, for the second term on the right hand side of (36), we have

$$\|\text{div}(c_i^K \mathbf{N}_i^K)\|_{0, \Omega} \leq C \delta_1.$$

For the estimation of the first term on the right hand side of (36), we have

$$(37) \quad \begin{aligned} \|\mathbf{u} - c_i^K \mathbf{N}_i^K\|_{0, K} &\leq \|\mathbf{u} - A(\mathbf{x}) \mathbf{u}^{sp}\|_{0, K} + \|A(\mathbf{x}) \mathbf{u}^{sp} - c_i^K \mathbf{N}_i^K\|_{0, K} \\ &\leq \|\mathbf{u} - A(\mathbf{x}) \mathbf{u}^{sp}\|_{0, K} + \|(A(\mathbf{x}) - \bar{A}_K) \mathbf{u}^{sp}\|_{0, K} + \|\bar{A}_K \mathbf{u}^{sp} - A_i \beta_i^K \mathbf{N}_i^K\|_{0, K} \\ &\leq \|\mathbf{u} - A(\mathbf{x}) \mathbf{u}^{sp}\|_{0, K} + \|A(\mathbf{x}) - \bar{A}_K\|_{\infty, K} \|\mathbf{u}^{sp}\|_{0, K} + \|(\bar{A}_K - A_i) \beta_i^K \mathbf{N}_i^K\|_{0, K} \\ &\leq \|\mathbf{u} - A(\mathbf{x}) \mathbf{u}^{sp}\|_{0, K} + \|A(\mathbf{x}) - \bar{A}_K\|_{\infty, K} \|\mathbf{u}^{sp}\|_{0, K} + C |\bar{A}_K - A_i| h, \end{aligned}$$

where  $\bar{A}_K$  is the mean of  $A_i$ . Here, we have taken into account that  $|\beta_i| \leq Ch$ , Proposition 4.2 and  $\|\mathbf{N}_i^K\|_{0, K} \leq C$  [13, 22] (the proof and a generalized version of the estimate for velocity basis function can be found in [2]). Summing (37) over all  $K$  and taking into account  $A(\mathbf{x}) \in C^\gamma$ , we have

$$\|\mathbf{u} - c_i \mathbf{N}_i\|_{0, \Omega} \leq C \delta + Ch^\gamma.$$

Thus, we have the following estimate

$$\|\mathbf{u} - c_i^K \mathbf{N}_i^K\|_{H(\text{div}, \Omega)} \leq C \delta + C \delta_1 + Ch^\gamma.$$

According to (27), for those  $K$  with  $\partial K \cap \partial \Omega \neq \emptyset$ , we will adjust proper  $c_i^K$  such that  $c_i^K \mathbf{N}_i^K - \mathbf{g}_{0, h} \in \mathbf{V}_h^0$ , but this adjustment will not affect our convergence rate. As for pressure approximation, choosing  $q_h = \langle p \rangle_K$  in each  $K$ , where  $\langle \cdot \rangle_K$  denotes the average over  $K$ , we use Poincare-Friedrichs inequality and obtain an estimate for the second term on right hand side of (27) by  $Ch$  (cf. [13]). Then we have the following theorem.

**Theorem 4.3.** *Assume (32) and (35) and  $A(\mathbf{x}) \in C^\gamma$ . Let  $(\mathbf{u}, p)$  and  $(\mathbf{u}_h, p_h)$  respectively solve the problem (22) and (24) with single-phase flow based mixed multiscale finite element, then*

$$(38) \quad \|\mathbf{u} - \mathbf{u}_h\|_{H(\text{div}, \Omega)} + \|p - p_h\|_{0, \Omega} \leq C\delta + C\delta_1 + Ch^\gamma + Ch.$$

## 5. Numerical Results

In this section, we present numerical results for permeability fields from SPE Comparative Solution Project [15] (also known as SPE 10). These permeability fields have channelized structure and a large contrast. Because of channelized structure of the permeability fields, the localized approaches do not perform well. We will show that if one uses of limited global information based on single-phase flow information in constructing multiscale basis functions, then the numerical approximation on the coarse grid becomes more accurate.

In our numerical results, we consider two-phase flow and transport as formulated in Section 2. We compare the saturation fields and water-cut data as a function of pore volume injected (PVI). The water-cut is defined as the fraction of water in the produced fluid and is given by  $q_w/q_t$ , where  $q_t = q_o + q_w$ , with  $q_o$  and  $q_w$  being the flow rates of oil and water at the production edge of the model. In particular,  $q_w = \int_{\partial\Omega^{out}} f(S)\mathbf{v} \cdot \mathbf{n} ds$ ,  $q_t = \int_{\partial\Omega^{out}} \mathbf{v} \cdot \mathbf{n} ds$ , where  $\partial\Omega^{out}$  is the outer flow boundary. Pore volume injected, defined as  $PVI = \frac{1}{V_p} \int_0^t q_t(\tau) d\tau$ , with  $V_p$  being the total pore volume of the system, provides the dimensionless time for the displacement. The permeability field  $k(\mathbf{x})$  is given on  $60 \times 220$  fine grid and different coarse grids are used in two-phase flow simulations without updating basis functions. We consider a traditional quarter five-spot problem (e.g., [1]), where the water is injected at left top corner and oil is produced at the right lower corner of the rectangular domain. In all numerical simulations, mixed multiscale basis functions are constructed once in the beginning of the computations.

In our simulations, we consider  $6 \times 10$ ,  $12 \times 11$  and  $12 \times 22$  coarse grids and pick three different layers, layer 40, 50 and 70, of SPE 10. For these cases, we compare the relative water-cut error (in  $L_2$ ) and the relative saturation error (in  $L_1$ ) by utilizing the local mixed MsFEM and the mixed MsFEM using limited global information from single phase flow. Table 2, 3, 4 show the numerical values of the relative water-cut errors and relative saturation errors for different coarse grids and layers. In the tables MMsFem stands for mixed MsFEM. In these numerical results, the viscosity ratio is taken to be  $\frac{\mu_w}{\mu_o} = \frac{1}{3}$ . One can observe from these tables that the errors of MsFEM using limited global information is almost an order of magnitude smaller than those for MsFEM using only local information. Moreover, MsFEM using limited global information converges as the coarse mesh size decreases, while MsFEM using local information does not converge and exhibits the resonance error. In Tables 5, 6 and 7, we present the relative water-cut and the relative saturation errors for high viscosity ratio  $\frac{\mu_w}{\mu_o} = \frac{1}{10}$ . These numerical results are consistent with those for lower viscosity ratio. Though the accuracy of MsFEM with global information deteriorates slightly, it is still more accurate compared to MsFEM with local information and converges as the mesh size decreases.

In Figure 2, the saturation profiles at  $PVI = 1$  for layer 50 are compared. The simulations are run with  $12 \times 11$  coarse grid and  $\frac{\mu_w}{\mu_o} = 1/3$ . It is evident from this figure that MsFEM using global information captures the fine-scale features accurately. On the other hand, local MsFEM solution is not very accurate. In Figure 3, the relative saturation errors from  $PVI = 0$  to  $PVI = 1$  are plotted. This figure clearly demonstrates that MsFEM using global information is accurate

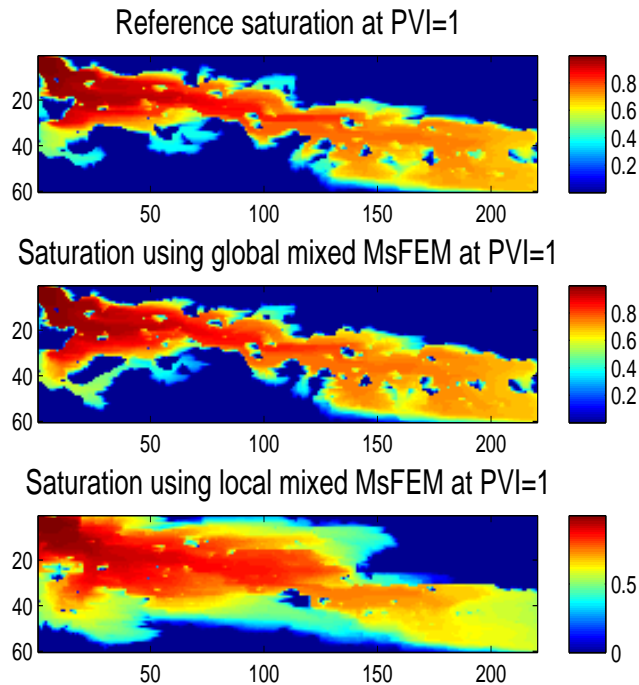


FIGURE 2. Comparison of saturation between reference solution and MsFEM solution at  $PVI = 1$ , layer=50,  $12 \times 11$  coarse grid and  $\frac{\mu_w}{\mu_o} = 1/3$ ; Top: The reference saturation; Middle: The saturation using global mixed MsFEM; Bottom: Multiscale saturation using local mixed MsFEM.

throughout the simulation. Figure 4 provides the comparison of water-cut curves between the reference, local mixed MsFEM and global mixed MsFEM. We observe that there is almost no difference between the reference and global mixed MsFEM water-cut curves. These observations are consistent for all other layers, coarse grids and viscosity ratios  $\frac{\mu_w}{\mu_o}$ . For example, in Figures 5, 6, and 7, we present the saturation profiles at  $PVI = 1$ , saturation errors and water-cut curves for the case  $\frac{\mu_w}{\mu_o} = 1/10$ .

It is clear from these figures that the use of the global information in mixed multiscale finite element methods gives us more accurate approximation. The presented numerical results convincingly show that one can use a single phase flow solution to construct basis functions that can be employed for solving two-phase flow and transport on the coarse grid accurately.

Next, we discuss the convergence of global mixed MsFEM with limited global information. For this reason, we consider different coarse grids,  $6 \times 10$ ,  $12 \times 11$ , and  $12 \times 22$  for the previous examples. As our convergence analysis indicates that the proposed method converges upto a small parameter  $\delta$  which represents how well two-phase velocity field can be approximated by single-phase velocity field in each coarse patch. Table 2 - 7 show that as the coarse mesh size decreases the error decreases. This confirms our convergence analysis for the global MsFEM. We note

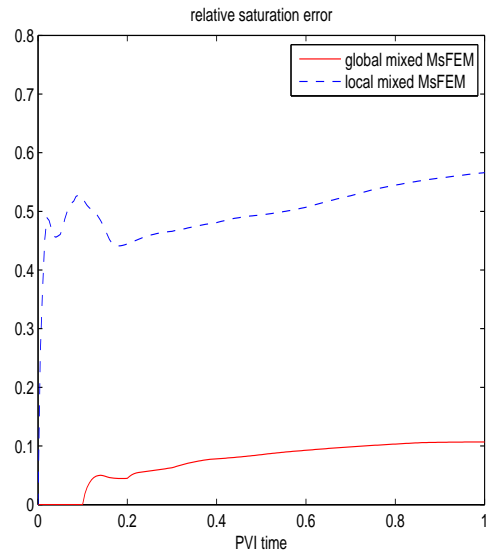


FIGURE 3. Relative saturation error, layer=50,  $12 \times 11$  coarse grid and  $\frac{\mu_w}{\mu_o} = 1/3$

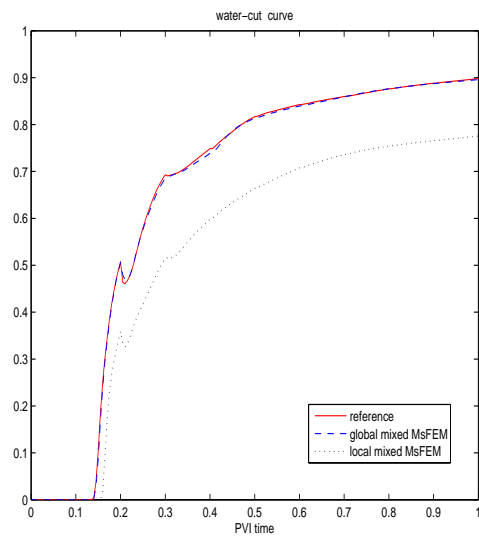


FIGURE 4. Water-cut curve, layer=50,  $12 \times 11$  coarse grid and  $\frac{\mu_w}{\mu_o} = 1/3$

that this is in contrast to standard MsFEM where one can observe the resonance error in the form  $\epsilon/h$ . As a result, the standard mixed MsFEM does not converge as  $h$  approaches to zero. More numerical results can be found in [22].

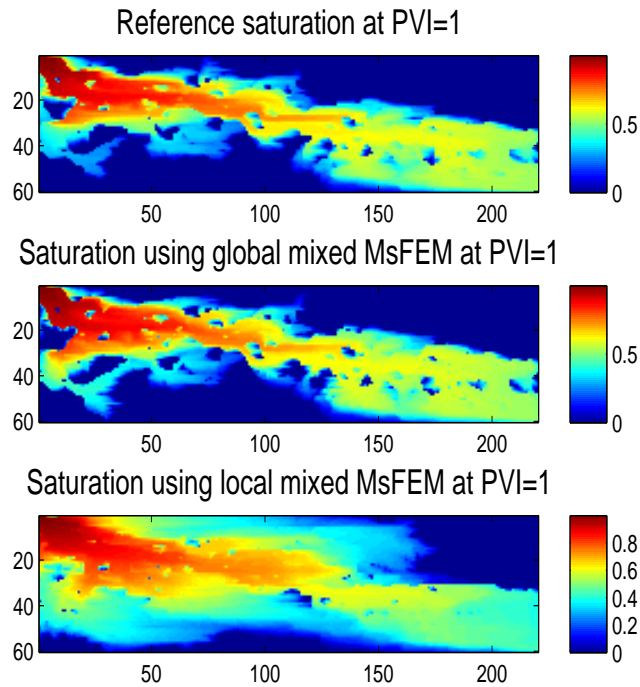


FIGURE 5. Comparison of saturation between reference solution and MsFEM solution at  $PVI = 1$ , layer=50,  $12 \times 11$  coarse grid and  $\frac{\mu_w}{\mu_o} = 1/10$ ; Top: The reference saturation; Middle: The saturation using global mixed MsFEM; Bottom: Multiscale saturation using local mixed MsFEM.

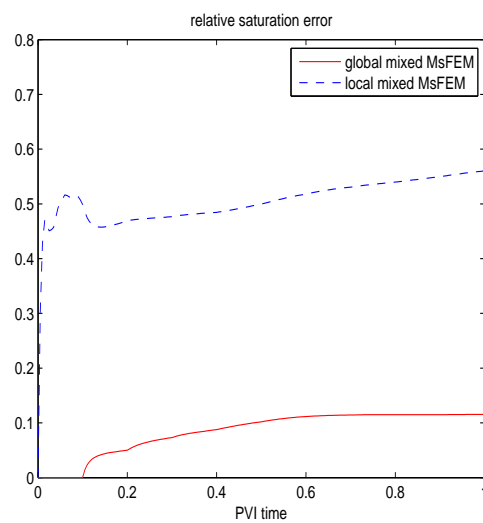


FIGURE 6. Relative saturation error, layer=50,  $12 \times 11$  coarse grid and  $\frac{\mu_w}{\mu_o} = 1/10$

TABLE 2. Relative Errors (layer=40,  $\frac{\mu_w}{\mu_0} = 1/3$ )

coarse grid	water-cut error global MMs fem	saturation error global MMs fem	water-cut error local MMs fem	saturation error local MMs fem
$6 \times 10$	0.0144	0.0512	0.1172	0.2755
$12 \times 11$	0.0093	0.0435	0.2057	0.3459
$12 \times 22$	0.0039	0.0370	0.1867	0.3158

TABLE 3. Relative Errors (layer=50,  $\frac{\mu_w}{\mu_0} = 1/3$ )

coarse grid	water-cut error global MMs fem	saturation error global MMs fem	water-cut error local MMs fem	saturation error local MMs fem
$6 \times 10$	0.0129	0.0871	0.1896	0.5061
$12 \times 11$	0.0055	0.0753	0.1806	0.5032
$12 \times 22$	0.0046	0.0568	0.1702	0.4578

TABLE 4. Relative Errors (layer=70,  $\frac{\mu_w}{\mu_0} = 1/3$ )

coarse grid	water-cut error global MMs fem	saturation error global MMs fem	water-cut error local MMs fem	saturation error local MMs fem
$6 \times 10$	0.0106	0.0562	0.0408	0.2291
$12 \times 11$	0.0081	0.0483	0.0863	0.2858
$12 \times 22$	0.0039	0.0421	0.0976	0.2530

TABLE 5. Relative Errors (layer=40,  $\frac{\mu_w}{\mu_0} = 1/10$ )

coarse grid	water-cut error global MMs fem	saturation error global MMs fem	water-cut error local MMs fem	saturation error local MMs fem
$6 \times 10$	0.0080	0.0534	0.0902	0.2721
$12 \times 11$	0.0056	0.0491	0.1382	0.3472
$12 \times 22$	0.0026	0.0403	0.1414	0.3153

TABLE 6. Relative Errors (layer=50,  $\frac{\mu_w}{\mu_0} = 1/10$ )

coarse grid	water-cut error global MMs fem	saturation error global MMs fem	water-cut error local MMs fem	saturation error local MMs fem
$6 \times 10$	0.0049	0.0957	0.1577	0.5137
$12 \times 11$	0.0042	0.0850	0.1499	0.5063
$12 \times 22$	0.0041	0.0628	0.1404	0.4613

TABLE 7. Relative Errors (layer=70,  $\frac{\mu_w}{\mu_0} = 1/10$ )

coarse grid	water-cut error global MMs fem	saturation error global MMs fem	water-cut error local MMs fem	saturation error local MMs fem
$6 \times 10$	0.0044	0.0629	0.0280	0.2262
$12 \times 11$	0.0027	0.0522	0.0576	0.2736
$12 \times 22$	0.0025	0.0473	0.0678	0.2397

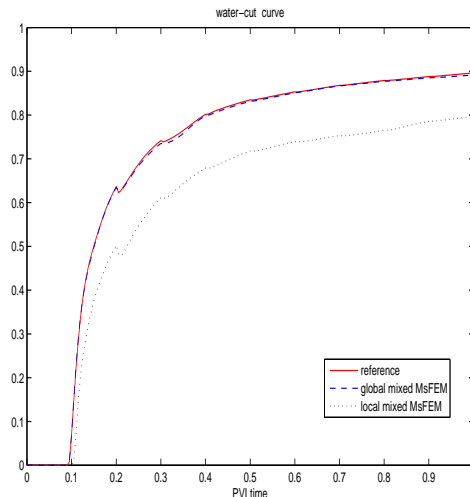


FIGURE 7. Water-cut curve, layer=50,  $12 \times 11$  coarse grid and  $\frac{\mu_w}{\mu_o} = 1/10$

## 6. Conclusions

In this paper, we present analysis and numerical results of multiscale finite element methods. These methods employ limited global information from the solution of a single-phase flow problem to construct accurate solutions of two-phase immiscible flow in heterogeneous porous media. Our analysis assumes that the fine-scale features of two-phase flow dynamics strongly depend on the single-phase flow. Under this assumption, we derive convergence rate for multiscale finite element methods. Our numerical results show that MsFEMs using single-phase information give more accurate results and converge as the coarse mesh size decreases.

## Acknowledgments

L. Jiang would like to acknowledge a support from Chinese NSF 10901050. J. E. Aarnes was funded by the Research Council of Norway under grant no. 158908/I30. Y. Efendiev would like to acknowledge a partial support from NSF grants DMS-0327713 and DOE grant DE-FG02-05ER25669. Efendiev's work was also partially supported by Award Number KUS-CI-016-04, made by King Abdullah University of Science and Technology (KAUST).

## References

1. J. AARNES, *On the use of a mixed multiscale finite element method for greater flexibility and increased speed or improved accuracy in reservoir simulation*, Multiscale Model. Simul., 2 (2004), pp. 421–439.
2. J. AARNES, Y. EFENDIEV, L. JIANG, *Mixed multiscale finite element methods using limited global information*, Multiscale Model. Simul., 7 (2008), pp. 655–676.
3. R. A. ADAMS, *Sobolev spaces*, Academic Press, New York-London, 1975. Pure and Applied Mathematics, Vol. 65.
4. T. ARBOGAST, *Implementation of a locally conservative numerical subgrid upscaling scheme for two-phase Darcy flow*, Comput. Geosci., 6 (2002), pp. 453–481.
5. T. ARBOGAST AND K. BOYD, *Subgrid upscaling and mixed multiscale finite elements*, SIAM J. Numer. Anal. 44 (2006), pp. 1150–1171.

6. M. AVELLANEDA AND F.-H. LIN, *Compactness methods in the theory of homogenization*, Comm. Pure Appl. Math., 40 (1987), pp. 803–847.
7. I. BABUŠKA, G. CALOZ, AND E. OSBORN, *Special finite element methods for a class of second order elliptic problems with rough coefficients*, SIAM J. Numer. Anal., 31 (1994), pp. 945–981.
8. BABUŠKA, I. AND MELENK, J. M., *The partition of unity method*, Internat. J. Numer. Methods Engrg., 40 (4), 1997, pp. 727–758
9. I. BABUŠKA AND E. OSBORN, *Generalized finite element methods: Their performance and their relation to mixed methods*, SIAM J. Numer. Anal., 20 (1983), pp. 510–536.
10. F. BREZZI, *Interacting with the subgrid world*, in Numerical analysis 1999 (Dundee), Chapman & Hall/CRC, Boca Raton, FL, 2000, pp. 69–82.
11. F. BREZZI AND M. FORTIN, *Mixed and hybrid finite element methods*, Springer-Verlag, Berlin – Heidelberg – New-York, 1991.
12. Y. CHEN, L. J. DURLLOFSKY, M. GERRITSEN, AND X. H. WEN, *A coupled local-global up-scaling approach for simulating flow in highly heterogeneous formations*, Advances in Water Resources, 26 (2003), pp. 1041–1060.
13. Z. CHEN AND T. Y. HOU, *A mixed multiscale finite element method for elliptic problems with oscillating coefficients*, Math. Comp., 72 (2002), pp. 541–576 (electronic).
14. P. G. CIARLET, *The finite element method for elliptic problems*, Horth-Holland, Amsterdam, 1978.
15. M. CHRISTIE AND M. BLUNT, *Tenth spe comparative solution project: A comparison of up-scaling techniques*, SPE Reser. Eval. Eng., 4 (2001), pp. 308–317.
16. Y. EFENDIEV, V. GINTING, T. HOU, AND R. EWING, *Accurate multiscale finite element methods for two-phase flow simulations*, J. Comput. Phys., 220 (1), pp. 155–174, 2006.
17. Y. EFENDIEV, T. HOU, AND V. GINTING, *Multiscale finite element methods for nonlinear problems and their applications*, Comm. Math. Sci., 2 (2004), pp. 553–589.
18. Y. EFENDIEV AND A. PANKOV, *Numerical homogenization of nonlinear random parabolic operators*, Multiscale Model. Simul., 2(2) (2004), pp. 237–268.
19. T. Y. HOU AND X. H. WU, *A multiscale finite element method for elliptic problems in composite materials and porous media*, J. Comput. Phys., 134 (1997), pp. 169–189.
20. T. HUGHES, G. FEIJOO, L. MAZZEI, AND J. QUINCY, *The variational multiscale method - a paradigm for computational mechanics*, Comput. Methods Appl. Mech. Engrg, 166 (1998), pp. 3–24.
21. P. JENNY, S. H. LEE, AND H. TCHELEPI, *Multi-scale finite volume method for elliptic problems in subsurface flow simulation*, J. Comput. Phys., 187 (2003), pp. 47–67.
22. L. JIANG, *Multiscale numerical methods using limited global information and their applications*, Ph.D. thesis, Texas A&M University, 2008.
23. L. JIANG, Y. EFENDIEV AND I. MISHEV, *Mixed multiscale finite element methods using approximate global information based on partial upscaling*, Comput. Geosci. 14 (2010), pp. 319–341.
24. V. V. JIKOV, S. M. KOZLOV, AND O. A. OLEINIK, *Homogenization of differential operators and integral functionals*, Springer-Verlag, New York, 1994.
25. A.-M. MATACHE AND C. SCHWAB, *Homogenization via p-FEM for problems with microstructure*, in Proceedings of the Fourth International Conference on Spectral and High Order Methods (ICOSAHOM 1998) (Herzliya), vol. 33, 2000, pp. 43–59.
26. G. SANGALLI, *Capturing small scales in elliptic problems using a residual-free bubbles finite element method*, Multiscale Model. Simul., 1 (2003), pp. 485–503.

College of Mathematics and Computer Science, Hunan Normal University, Changsha, 410081, China; IMA, University of Minnesota, Minneapolis, MN 55455  
*E-mail:* [lijiang@ima.umn.edu](mailto:lijiang@ima.umn.edu)

Det Norske Veritas AS, Veritasveien 1, 1322 Høvik, Norway  
*E-mail:* [Jorg.Aarnes@dnv.com](mailto:Jorg.Aarnes@dnv.com)

Department of Mathematics, Texas A&M University, College Station, TX, 77840  
*E-mail:* [efendiev@math.tamu.edu](mailto:efendiev@math.tamu.edu)